# Internal Probe Studies of a Low Voltage Hall Thruster

**IEPC-2019-A-932**

*Presented at the 36th International Electric Propulsion Conference*
*University of Vienna, Austria*
*September 15-20, 2019*

Jerry L. Ross*
*East Stroudsburg University, East Stroudsburg, PA, 18301, USA*

**Efficient, low voltage Hall thrusters offer the potential to operate as a primary and auxillary propulsion system. Low voltage operation necessary to achieve the required high thrust-to-power ratio has previously resulted in a reduced thrust efficiency that has been difficult to correct. In this study, internal probe studies of a traditional BPT-2000 Hall Thruster are taken as a function of discharge voltage and supplied magnetic current with the aim to identify mitigating factors of low efficiency. Among the internal probe results, it was found that the ionization zone moves upstream with respect to the acceleration region with decreased magnet current for low voltages. This resulted in an increase in voltage utilization efficiency. Decreasing the magnet current was shown to increase the peak ion density and shift the entire ion density profile further upstream for low voltage operation.**

## Nomenclature

| | |
|---|---|
| $T$ | = thrust, N |
| $U_e$ | = ion velocity, m/s$^2$ |
| $\Delta t$ | = trip time, s |
| $M$ | = spacecraft mass, kg |
| $m$ | = mass of a propellant atom/ion, kg |
| $V_d$ | = discharge voltage (anode potential), V |
| $\epsilon_{ion}$ | = ion kinetic energy |
| $\eta_{probe}$ | = the product of all probe-measured efficiencies |
| $V_{accel}$ | = acceleration potential for a given ion, V |
| $\eta_v$ | = voltage utilization efficiency |
| $\eta_T$ | = thrust efficiency |
| $I_i$ | = exhausted ion current, A |
| $I_d$ | = discharge current, A |
| $e$ | = elementary charge, C |
| $P_s$ | = supply output power $I_d V_d$, W |
| $T_e$ | = electron temperature, J |
| $m_i$ | = ion mass, kg |
| $m_e$ | = electron mass, kg |
| $m_p$ | = mass of the power supply, kg |
| $k$ | = Boltzmann constant, m$^2$ kg s$^{-2}$ K$^{-1}$ |
| $I_{sat}$ | = ion saturation current, A |
| $n_i$ | = ion density, m$^{-3}$ |

*Associate Professor, Physics, jross@esu.edu.

## I. Introduction

Within the electric propulsion community there are many efforts to utilize EP devices that can function both as a primary and auxiliary device for a spacecraft. The benefits of a single mulit-purposed propulsion system include reducing complexity (increased reliability) and reduction of the total system mass. Such a system requires an increase in thrust output. Ostensibly, increasing the thrust becomes can be accomplished by increasing the power supplied to the thruster. However, unlike in a chemical thruster where this power comes from the energy stored in the chemical bonds of the propellant, an electrical thruster gets its power from an onboard power plant (PPU) that converts solar or nuclear energy into electricity. Available onboard power from PPUs are limited at present to tens of kW which limits the thrust of EP devices to at present to hundreds of mN. Furthermore, the mass of the PPU scales with its power output,

$$P_s = \quad \propto m_p = \frac{2\eta_T T}{U_e}. \tag{1}$$

By increasing the onboard power supply, the total expended propellent mass needed for the mission, $\Delta m$, is decreased, while the $m_p$ is increased. Thus, missions are designed to minimize $m_p + \Delta m$ to maximize the deliverable payload.[1]

Without the ability to increase the onboard power, focus must move toward trying to increase the thrust-to-power ratio,

$$\frac{T}{P_s} = \frac{2\eta_T}{U_e}, \tag{2}$$

which means either decreasing the exit velocity or increasing the thrust efficiency.

In the past, there has been great progress in increasing thrust efficiencies from benchmark levels of 50% on the Russian SPT-100 to upwards of 70% in some laboratory Hall thrusters.[2,3] However, for many missions where EP could be considered, a several fold increase in thrust is necessary where even perfect thrust efficiency will not increase the thrust-to-power ratio to necessary levels.

Alternatively, according the equation 2, decreasing the propellant exit velocity will cause an increase in the thrust to power ratio for a fixed thrust efficiency. The propellant exit velocity is related to the the acceleration voltage by

$$\frac{1}{2} m U_e^2 = q V_{accel}, \tag{3}$$

where $V_{accel}$ is approximately the voltage applied to the anode

$$V_{accel} \approx V_d. \tag{4}$$

Unfortunately, decreasing the voltage applied to the anode (discharge voltage) on modern Hall thrusters has resulted in decreases in thrust efficiency, $\eta_T$. Experimental data has shown that the decrease is so severe, that the thrust-to-power ratio declines instead of increasing. Thus, the problem of a high thrust-to-power ratio reverts back to increasing, or maintaining, the thrust efficiency at low discharge voltages.

There is a large gap in the empirical data available for low voltage operation of Hall thrusters. As a fledging technology, it was discovered that Hall thrusters did not perform well at voltages below $\sim 300$ V. Therefore, experiments were focused on the areas where the device performed the best, namely, high voltages. Although some of the loss mechanisms of low voltage have been identified, many have not. To further complicate matters, some of the data available exhibit non-monotonic behavior that is not conventionally explained by the models used in the field.

In 2003, Manzella experimented on the NASA-120M and NASA-457M Hall thrusters and narrowed the leading loss mechanism to voltage utilization efficiency or ionization efficiency of low voltage operation. The devices in the aforementioned study were operated as low as 100 V on the anode at $< 25\%$ efficiency.[4] The study achieved upwards of 80 mN/kW with the larger of the two thrusters the 457M. The data included thrust measurements, mass flow settings, and discharge power supply readings. With this information, the ionization fraction and exit velocity are indeterminate. Hence, the loss mechanisms can only be postulated without probe data.

More recently, extensive testing of the performance of low voltage Hall thrusters was conducted by Dan Brown.[5] Brown used a 6 kW laboratory thruster to perform exhaustive probe and thrust stand measurements for discharge voltages of 300 V down to 105 V at both 20 mg/s and 10 mg/s propellant flow rates. At 20 mg/s, Brown showed a maximum thrust-to-power of 86.4 mN/kW at a discharge voltage of 120 V. At 100

V $V_d$ the ratio dropped as the thrust efficiency fell from 41% to 34%. The recycled electron current was the dominant loss mechanism at 71% current efficiency. The voltage utilization efficiency, however, saw the greatest change, -14%, when the discharge voltage was reduced from the nominal 300 V down to 105 V.

In the 10 mg/s case, the maximum thrust-to-power was 85.5 mN/kW and the current efficiency was also the dominant loss mechanism. Here, current efficiency exhibited the greatest change, -16%, from the nominal discharge voltage at this flow rate. All measurements in all test cases were taken at maximum thrust efficiency for a given discharge voltage. Which is to say, all measurements were taken at a single magnet current level.

In the preceding study to this one, it was concluded that voltage utilization efficiency was increasing with decreasing magnet current.[6] This indicated that the plasma acceleration region and/or ionization zone may have moved in axial direction. In order to find out, the electron temperature, floating potential, and plasma potential as a function of the axial direction are needed. Furthermore, since most of the physics of interest happen very close to the anode, measurements will have to include axial locations within the discharge chamber.

This work expands the experimental data for low voltage operation by examining plasma processes inside the discharge chamber by using internal Langmuir probe sweeps. To broaden the results of these experiments, all the experiments were conducted using both xenon and krypton as propellant sources.

Therefore, this experiment designed a system capable of internal probe messurements that allow for a more in depth understanding of the acceleration and ionization processes seen in the low voltage thrusters.

## II. Design of the High-Speed Probe System

A High-speed Probe System (HPS) was designed to obtain electron temperature, ion density, and plasma potential both outside and inside the discharge chamber. From these values, the acceleration zone and ionization zone can be determined for low voltage and low magnet current operation. The system includes the motion table, the AC servo drive system, the double Langmuir probe and accompanying data acquisition system.

The design of the HPS was modeled from Haas' work in internal Hall thruster measurements.[7] From his work, the melting time of a probe within a plasma for various peak magnetic fields as a function of axial electric was determined.[8] The operating voltages in this study were 300 V and below, thus a 500 ms of residence time within the discharge chamber is permitted to avoid melting. In addition to ablation of the probe, plasma perturbation is always concern. The probe system was designed to record 18 mm of of depth into the discharge chamber, leaving a 2 mm buffer between the probe tip and the anode face, and achieved a total residence time of less than 60 ms. The current, voltage and floating potential of the double probe were collected for each millimeter of travel for a peak collection rate of 93.75 kHz. An optical encoder was used to determine the position of the probe and synced the data collection which was verified accurate to $\pm 0.3$mm. Additional details of the system can be found here[6]

### Operation Matrix

Table 1 lists the discharge voltages and mass flow rates included in the experiment. The original test plan included a 100 V discharge voltage trial for both propellants. In testing, the thruster struggled to remain on below 125 V. Since the successful test set of data for the 100 V case was largely incomplete, it has been omitted.

## III. Analysis

The presence of the magnetic field in the Hall thruster changes the shape of the sheath surrounding the probe. Since the ions remain unmagnetized, the ion saturation potential is used to calculate the ion density. The current collected by a double probe as a function of voltage is,

$$I(V) = I_{sat} \tanh\left(\frac{eV}{2kT_e}\right) \tag{5}$$

Table 1: Test parameters for xenon and krypton

(a) Xenon

| $V_d$ (V) | $I_m$ (A) | $\dot{m}$ (mg/s) |
|---|---|---|
| 300 | 3.00 | 5 |
| 300 | 2.50 | 5 |
| 300 | 2.00 | 5 |
| 300 | 1.50 | 5 |
| 300 | 1.00 | 5 |
| 200 | 3.00 | 5 |
| 200 | 2.50 | 5 |
| 200 | 2.00 | 5 |
| 200 | 1.50 | 5 |
| 200 | 1.00 | 5 |
| 150 | 3.00 | 5 |
| 150 | 2.50 | 5 |
| 150 | 2.00 | 5 |
| 150 | 1.50 | 5 |
| 150 | 1.25 | 5 |
| 150 | 1.00 | 5 |
| 150 | 0.75 | 5 |
| 150 | 0.50 | 5 |
| 125 | 2.00 | 5 |
| 125 | 1.50 | 5 |
| 125 | 1.25 | 5 |
| 125 | 1.00 | 5 |
| 125 | 0.75 | 5 |
| 125 | 0.50 | 5 |
| 125 | 0.25 | 5 |

(b) Krypton

| $V_d$ (V) | $I_m$ (A) | $\dot{m}$ (mg/s) |
|---|---|---|
| 300 | 3.00 | 5 |
| 300 | 2.50 | 5 |
| 300 | 2.00 | 5 |
| 300 | 1.50 | 5 |
| 300 | 1.00 | 5 |
| 200 | 3.00 | 5 |
| 200 | 2.50 | 5 |
| 200 | 2.00 | 5 |
| 200 | 1.50 | 5 |
| 200 | 1.25 | 5 |
| 200 | 1.00 | 5 |
| 200 | 0.75 | 5 |
| 150 | 3.00 | 5 |
| 150 | 2.50 | 5 |
| 150 | 2.00 | 5 |
| 150 | 1.50 | 5 |
| 150 | 1.25 | 5 |
| 150 | 1.00 | 5 |
| 150 | 0.75 | 5 |
| 150 | 0.50 | 5 |
| 125 | 1.25 | 5 |
| 125 | 1.00 | 5 |
| 125 | 0.75 | 5 |
| 125 | 0.50 | 5 |
| 125 | 0.25 | 5 |

where $I_{sat}$ is the ion saturation current.[9] Assuming a maxwellian temperature distribution within the plasma, a custom curve fit is constructed,

$$f(x) = A\tanh(Bx + E) + Cx + D \tag{6}$$

where $A, B, C, D$ and $E$ are the fit coefficients to be solved for. The linear portion of the curve fit $Cx$ accounts for the growing sheath (effective probe surface area) as the voltage is increased. By comparing equations 5 and 6 the coefficient $A$ is exactly the ion saturation current. Similarly, the electron temperature in electron volts is

$$T_e = \frac{1}{2B} \tag{7}$$

The "Bohm Current" or ion saturation current is equal to,

$$I_{sat} = n_i e A_s \sqrt{\frac{kT_e}{m_i}}, \tag{8}$$

where $n_i$ is the ion density (which is the same as the electron density due to quasineutrality), $A_s$ is the probe collecting surface area, $m_i$ is the ion mass.[10] Taking the ion saturation current from equation 6 and the electron temperature from equation 7 we can solve for the ion density with equation 8. The plasma potential is calculated as

$$V_p = V_f + \frac{T_{eV}}{2}\ln\left(\frac{2m_i}{\pi m_e}\right) \tag{9}$$

where $T_{eV}$ is the electron temperature in electron volts.[9]

This process was automated using a combination of Matlab and Igor Pro scripts to produce the following three parameters of interest for each double probe trace: electron temperature, electron density and plasma potential.

It was believed that the disturbance created in the plasma, by the presence of the probe, is less severe on the inward stroke than the outward stroke by simple virtue that the inwards stroke occurs first. Aside from asymmetries in the perturbations the dataset for the inward and outwards stroke should be identical. Thus, it was chosen analyze the inward bound portion of the sweep.

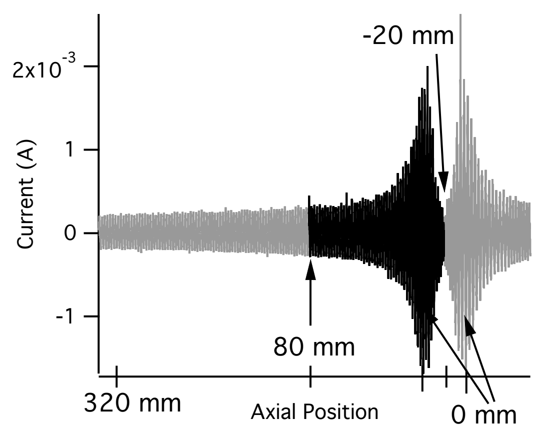


Figure 1: Raw current data as a function of axial position as recorded by the HPS. Only the portions in black were used for data analysis.

# IV. Results

## A. Xenon Results

Figures 2a - 5b represent a selection of the fully analyzed data to illustrate certain trends. To avoid obscuring the data error bars have been omitted from the graphs. Plasma potential, floating potential, electron energy and ion density are represented in red, green, black and blue, respectively. The sample set in figures 2a - 5b was chosen here to exhibit eight permutation samples of high/low discharge voltage, high/low magnet current, and propellant type.

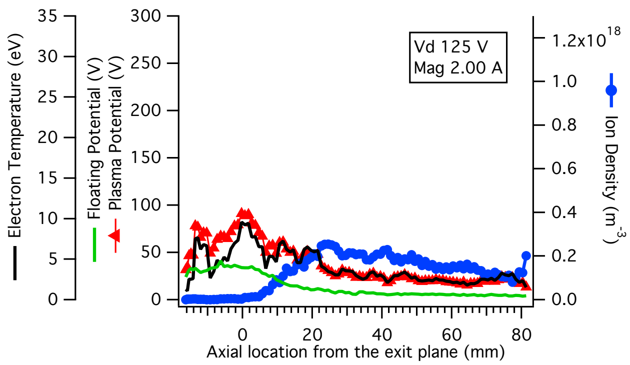


(a) High-speed probe data for xenon

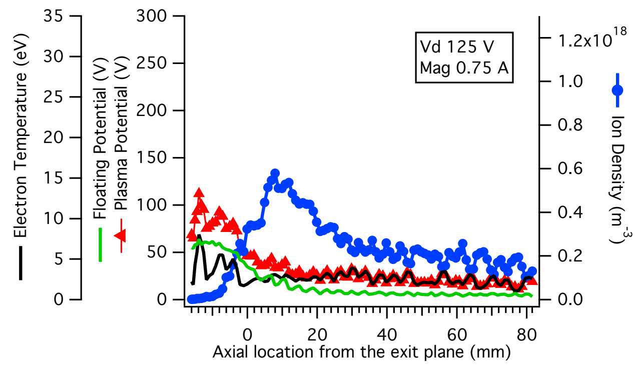


(b) High-speed probe data for xenon

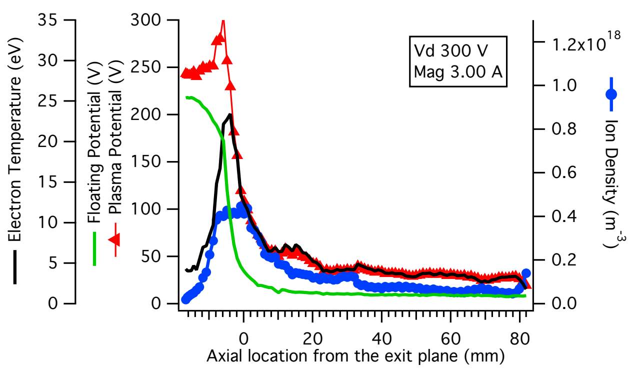


(a) High-speed probe data for xenon

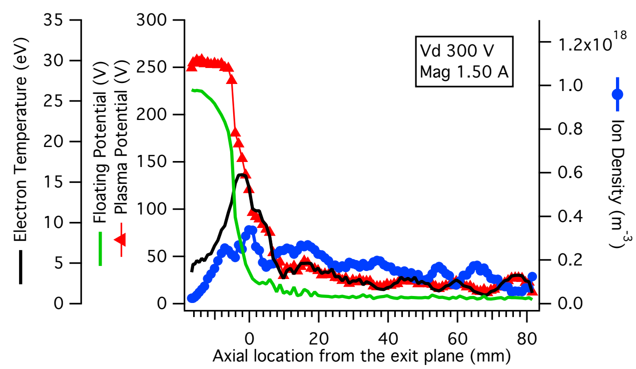


(b) High-speed probe data for xenon

## B. Krypton Results

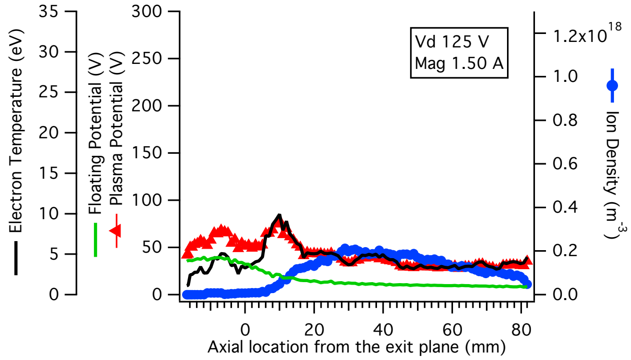


(a) High-speed probe data for krypton

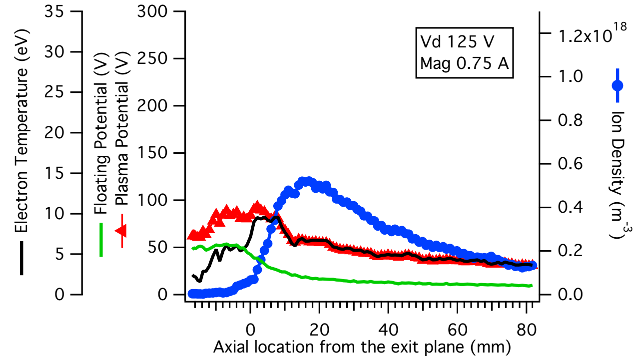


(b) High-speed probe data for krypton

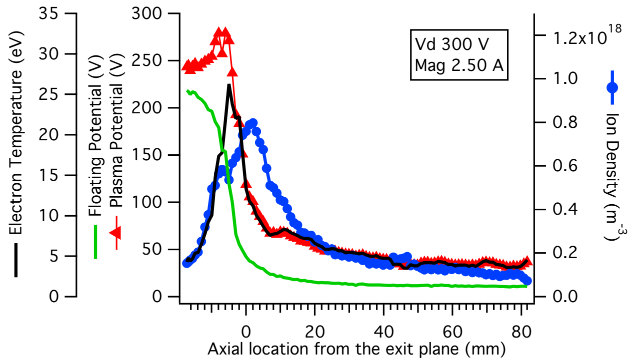


(a) High-speed probe data for krypton

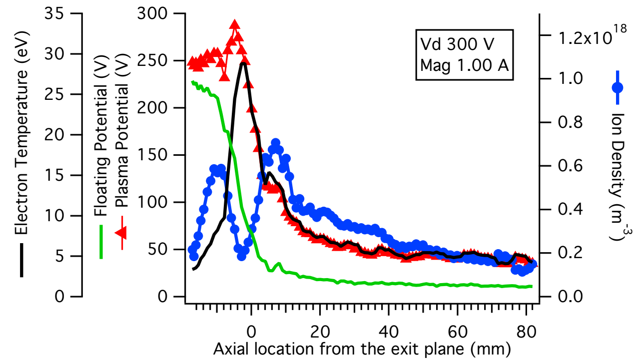


(b) High-speed probe data for krypton

### *1. Overall trends and shape*

The change in magnet current seems to have a greater effect on the ion densities than it does on the plasma potentials. For both xenon and krypton at 125 V, the higher magnet values push the maximum ion density further downstream such that the vast majority of the charged particles are outside of the discharge chamber. Very little ion density is recorded until about 5 mm past the exit plane for xenon and about 4 mm for krypton.

At 300 V, neither propellant shows much movement in the acceleration zone location as a function of magnet current. The ion densities exhibit opposite movement, in comparison to the 125 V cases for both propellants, with increased magnet current causing a downstream shift in the ion density profile. For xenon, the peak ion density moves from upstream of the exit plane to downstream of it. The same is true for krypton, but can be seen to be even more pronounced (figures 5a and 5b).

## C. Ionization and Acceleration Zone locations

In order to speak quantitatively on the effects of the magnet current on the plasma potential and ion density profiles, it is useful to mathematically define and identify what is known as the ionization zone and acceleration zone.

### *1. Ionization Zone*

Theoretically, the ionization zone is the axial location of peak ion production for the thruster. Experimentally, the ionization zone is identified by the point of maximum current density.[7,11,12] Although current density and ion production, as a function of axial distance, are closely related, the point of peak ion production can occur upstream of peak ion density. Ion density is a function of charged particle flux. Therefore, the ion density differs from ion production location by the additional current recorded due to downward streaming ions created upstream of the probe location. To record ion production location is to record only newly born ions or those of zero velocity (aside from random thermal motion), which is something these probe techniques are incapable of. The ionization zone locations, as determined by the peak ion density, can be found in tables 2 and 3.

Table 2: Krypton Ionization Zone. Values are given in mm from the exit plane. Negative values indicate locations internal to the discharge chamber.

| Magnet Current (A) | 125 V | 150 V | 200 V | 300 V |
|---|---|---|---|---|
| 0.50 | 16.2 | 9.2 | | |
| 0.75 | 17.2 | 9.2 | -1.8 | |
| 1.00 | 22.2 | -6.7 | -5.7 | 7.2 |
| 1.25 | 30.1 | 1.2 | -0.8 | |
| 1.50 | 29.1 | 0.2 | -1.8 | -7.7 |
| 2.00 | | -4.8 | -2.7 | 2.2 |
| 2.50 | | 29.1 | -3.8 | 2.2 |
| 3.00 | | 30.1 | -1.8 | 2.2 |

Table 3: Xenon Ionization Zone. Values are given in mm from the exit plane. Negative values indicate locations internal to the discharge chamber.

| Magnet Current (A) | 125 V | 150 V | 200 V | 300 V |
|---|---|---|---|---|
| 0.50 | 15.1 | 4.1 | | |
| 0.75 | 8.1 | 10.1 | | |
| 1.00 | 8.1 | 9.1 | 6.1 | 9.1 |
| 1.25 | 14.1 | 6.1 | | |
| 1.50 | 19.1 | 2.1 | 6.1 | 0.2 |
| 2.00 | 25.1 | 11.1 | 2.1 | 1.1 |
| 2.50 | | 18.1 | 3.1 | 1.1 |
| 3.00 | | 18.1 | 2.1 | -0.9 |

#### *2. Acceleration Zone*

The location of the acceleration zone can be identified by the point of steepest slope in the plasma potential profile. Mathematically, this can be located by taking the peak of the derivative of the plasma potential profile. Due to the uncertainty in the electron temperature measurements from which the plasma potential is derived (see equation 9), the results of this approach were highly erratic. Therefore, the acceleration zone location was determined using the same mathematical approach described above using the floating potential data. Numerous other works have taken this same approach due to the reliability of the floating potential data and its likeness to the plasma potential.[13–17] The results from the plasma potential data were then compared to the floating potential data to establish a level of measurement uncertainty. Removing extreme outliers, the acceleration zone as determined by floating potential was on average $\pm 2$ mm from the same calculation with the plasma potential data. The acceleration zone location results are in the tables 4 and 5.

Table 4: Krypton Acceleration region. Values are given in mm from the exit plane. Negative values indicate locations internal to the discharge chamber.

| Magnet Current (A) | 125 V | 150 V | 200 V | 300 V |
|---|---|---|---|---|
| 0.50 | -0.1 | -1.5 | | |
| 0.75 | 2.0 | 1.6 | -3.9 | |
| 1.00 | 3.1 | 3.0 | -4.1 | -3.9 |
| 1.25 | 3.0 | 1.8 | -2.6 | |
| 1.50 | 4.0 | 4.3 | -3.1 | -4.7 |
| 2.00 | | 5.3 | -3.3 | -4.9 |
| 2.50 | | 5.3 | -2.5 | -5.0 |
| 3.00 | | 6.8 | 2.9 | -4.8 |

Table 5: Xenon Acceleration Region. Values are given in mm from the exit plane. Negative values indicate locations internal to the discharge chamber.

| Magnet Current (A) | 125 V | 150 V | 200 V | 300 V |
|---|---|---|---|---|
| 0.50 | -3.2 | -4.9 | | |
| 0.75 | -0.1 | -3.8 | | |
| 1.00 | 0.8 | 1.2 | -2.2 | -2.6 |
| 1.25 | 4.6 | 3.8 | | |
| 1.50 | 5.7 | 4.1 | -2.4 | -4.1 |
| 2.00 | 9.6 | 5.7 | -3.2 | -4.0 |
| 2.50 | | 8.6 | -3.2 | -4.8 |
| 3.00 | | 7.7 | -3.1 | -3.9 |

### D. Potential Drop in the Acceleration Zone

In addition to the location of the ionization and acceleration zones, of equal importance to voltage utilization efficiency is the magnitude of the potential drop in the acceleration zone. This holds true, assuming any positively disproportionate amount of ion production occurs in the acceleration zone. For a given/fixed acceleration and ionization zone, if the maximum plasma potential in the acceleration zone is decreased, the voltage utilization efficiency will decrease. The potential drop can be calculated by subtracting the minimum plasma potential as found 20 mm downstream[a] from the exit plane from the maximum plasma potential inside the discharge chamber (or shortly outside of). The results are in figures 6 and 7 and it can be seen that the potential drop across the acceleration zone is minimally affected by the changing magnet current within the limits of the uncertainty.

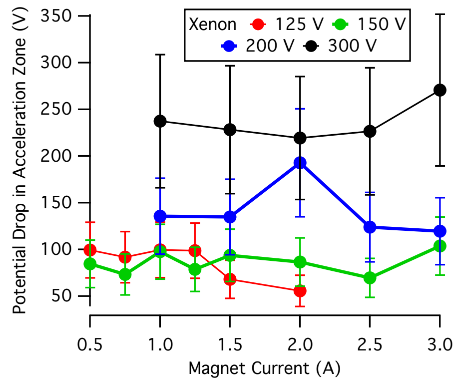


Figure 6: Potential drop across the acceleration zone for xenon

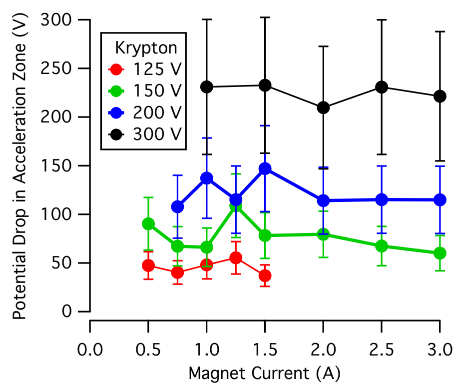


Figure 7: Potential drop across the acceleration zone for krypton

## V. Discussion

With the exception of a possible near-anode potential rise, it should not be possible for the plasma potential to be increasing as a function of axial distance from the anode in a Hall thruster. In many of our experimental cases, however, the results show the plasma potential increasing downstream of the anode all the way out to exit plane (see figure 5a). This is believed to be an artifact of the data, and is likely a byproduct of the uncertainty in the electron temperatures due to perturbation in the plasma caused by the insertion of the probe. The electron energy measurements have at 30% uncertainty which propagates to an uncertainty of anywhere between ±10 V to ±80 V in the calculation of the plasma potential. The

[a]The automated script actually searches for the minimum plasma potential value within ±3 mm from the 20 mm location to avoid any anomalous peaks

anomalous downstream rise in the plasma potential is therefore assumed to be the propagation of the electron temperature uncertainty. Figures 8 and 9 are example cases that display the plasma potential and its uncertainty plotted along side the floating potential and the electron temperature.

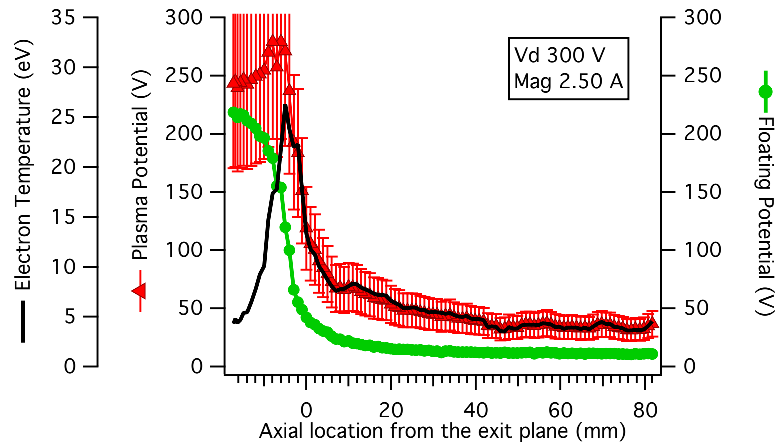


Figure 8: An example of floating potential, plasma potential and electron energy for krypton at 300 V

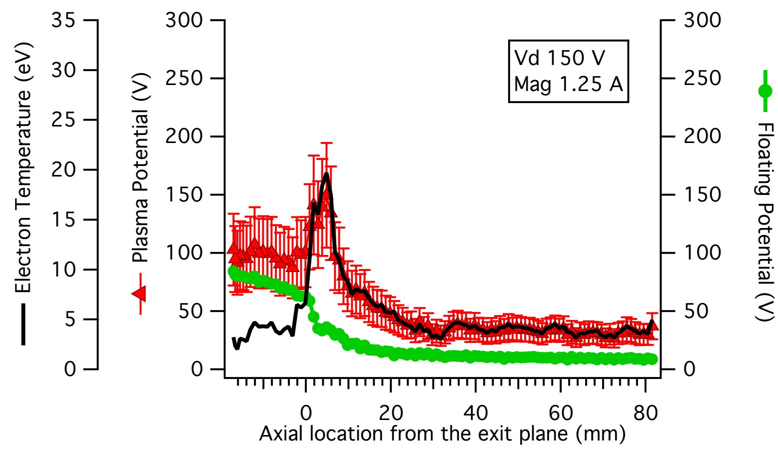


Figure 9: An example of floating potential, plasma potential and electron energy for krypton at 150 V

The ionization zone location is seen to be immobile for high voltages and magnet currents greater than 1.50 A for both propellants. The same can be said of the acceleration location. This indicates a lowered sensitivity in ion creation/acceleration dynamics on the magnetic field for nominal discharge voltages. In other words, axial position of the ionization processes are much more susceptible to changes in the magnetic field for low voltages than than they are for nominal/higher discharge voltages. This is in direct support of the external probe data found in other work.[6,18]

For both propellants, lowering the magnet current has the effect of increasing the plasma density and pushing it backward into the discharge chamber. Although the upstream shift is visually apparent in figures 10 and 11, the calculation of the ionization zone, seen in figures 15 and 17, does not show the same result. This is ramification of detecting the ionization zone by the peak in the ion density profile. For many cases, this is a solid approximation, however, for cases like xenon at 125 V with 0.50 A magnet current (figure 12), the peak of the ion density profile concludes that the ionization region is 15.1 mm downstream of the exit plane. Upon visual inspection of figure 12, it is clear that much of the ionization region occurs near the exit

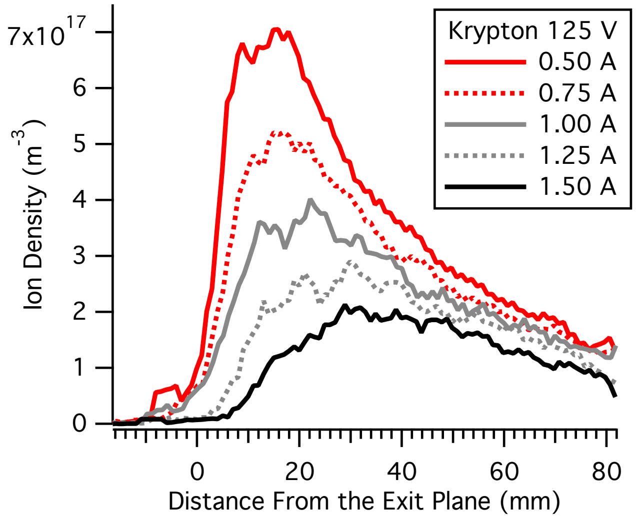


Figure 10: Krypton ion density

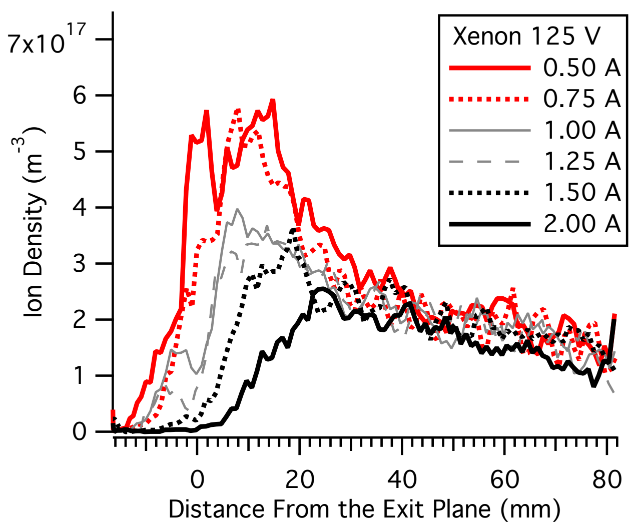


Figure 11: Xenon ion density

plane.

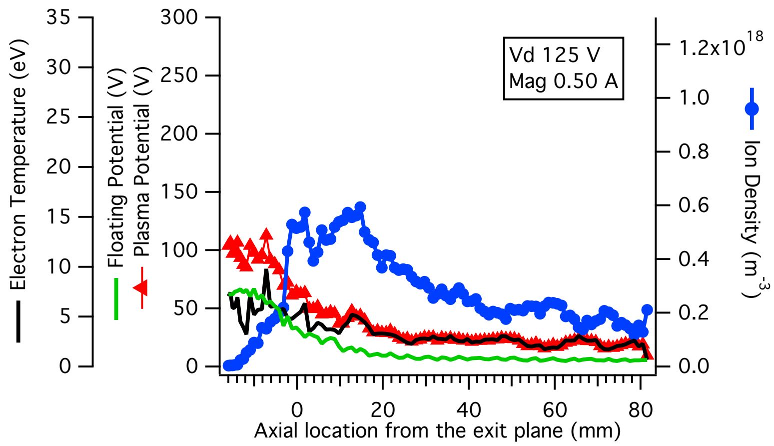


Figure 12: High-speed probe results for xenon at 125 V 0.50 A

In the experiments leading up to this work, it was shown that voltage utilization efficiency increases with decreasing magnet current for both propellants.[6,18] The voltage utilization of an ion is dependent on where it is ionized along the potential structure created by the anode-cathode voltage. Collisions will also have a small energy-robbing effect on an ion, but the bulk of an ion's exit velocity is determined by the portion of the anode potential it sees. There are only a few possibilities that would lead to an increase in voltage utilization:

- The potential drop in the acceleration zone could be increasing (assuming any portion of the ion production occurs in, or upstream, of the acceleration zone).
- The ionization zone is moving upstream with respect to the acceleration zone.

The latter hypothesis could involve both regions moving in either direction, upstream or downstream, but the net effect must be that the ionization zone is further upstream with respect to the acceleration zone to see an increase in the voltage utilization. Theses results discount the first hypothesis and support the second, see figures 14 - 17. Note that negative values indicate a distance in mm inside the discharge chamber from the exit plane and positive values are distances away from the exit plane.

The uncertainty in the acceleration location is taken to be $\pm$ 2 mm. The unknown error in the ionization zone location measurement arises from the fact that the peak ion density is not necessarily the location of peak ion production. Although it is reasonable to assume that the peak ion density marks the end of the ion production region, the peak of ion production could occur further upstream than the peak ion density. Therefore, as a conservative error estimate, if the distance is measured over which the ion density is increasing (ion production region), it can be assumed that the peak in ion production occurs in the later half of this distance. In other words, it is assumed that the ion production region begins inside the discharge chamber where the current density is non-trivial ($> 0.1\times10^{18}$ m$^{-3}$), and ends at the peak of the ion density profile.[b] Half of this distance is taken as the uncertainty in the ionization zone location as a one-sided error bar in the upstream direction from the stated ionization zone location. Figure 13 is a graphical example of the uncertainty region as determined by the above criteria. The resolution uncertainty due to the probe positioning system is less than 1 mm in either direction.

For most operating conditions, the beginning of the ion production region, as determined by the first downstream location from the anode of non-trivial current density $> 0.1\times10^{18}$ m$^{-3}$, begins at the closest location to the anode measured, -18 mm from the exit plane. This is not universal, however, as several of the low voltage cases do not show signs of significant ion production until further downstream towards the exit plane.

Table 6: The upstream uncertainty in the ionization zone location as measured from the peak ion density toward the anode

| Discharge Voltage | 125 V | 150 V | 200 V | 300 V |
|---|---|---|---|---|
| Xenon | 13 mm | 11 mm | 10 mm | 7 mm |
| Krypton | 13 mm | 10 mm | 7 mm | 9 mm |

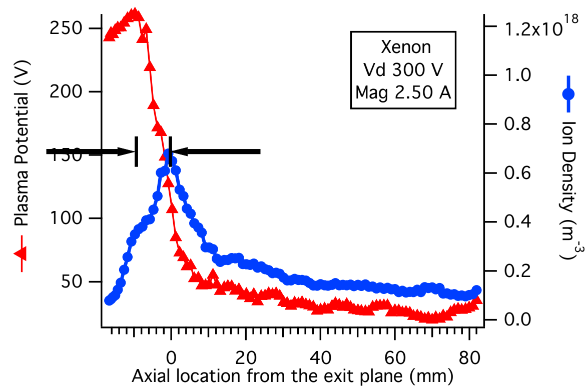


Figure 13: An example of the uncertainty in the ionization zone location as shown between the black arrows

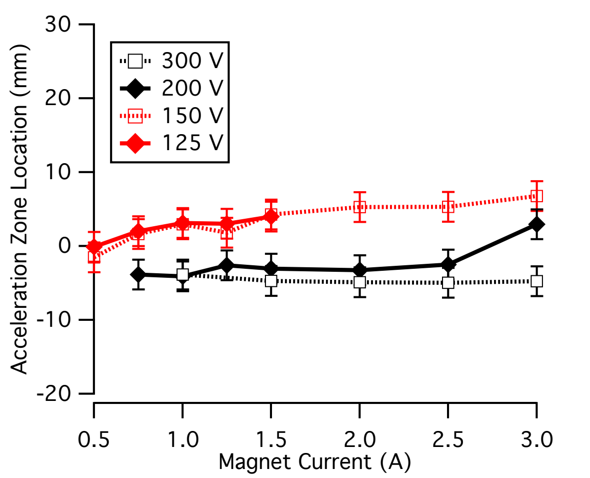


Figure 14: Acceleration zone location as a function of magnet current for krypton

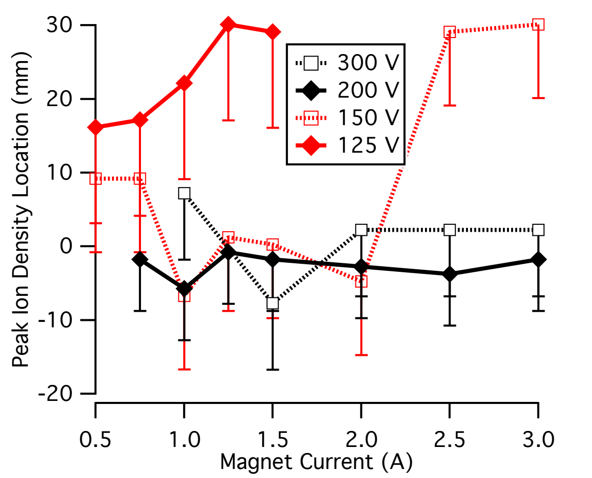


Figure 15: Ionization zone location as a function of magnet current for krypton

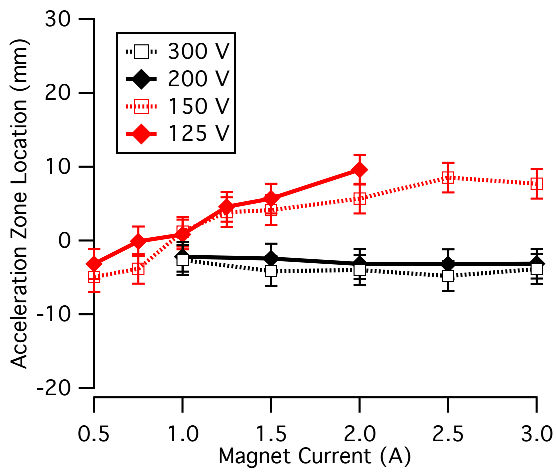


Figure 16: Acceleration zone location as a function of magnet current for xenon

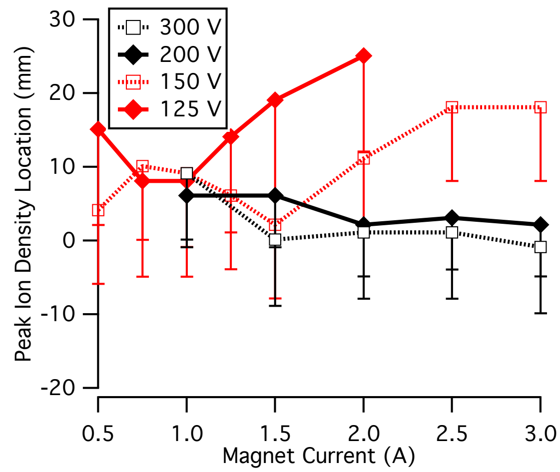


Figure 17: Ionization zone location as a function of magnet current for xenon

# VI. Conclusions

There is no appreciable change in the fraction of the discharge voltage drop in the acceleration zone as a function of magnet current for any discharge voltage as shown. As a function of magnet current, however, there is an axial shift in both the acceleration and ionization zone locations in the upstream direction for low voltage trials. This shift is greater for the ion density profile, driving the ionization zone upstream towards the anode.

For xenon at higher voltages, the acceleration zone location is moved upstream with decreasing magnet current for the 200 V case and and ever so slightly downstream in the 300 V case. For krypton, neither the 200 V or 300 V cases show much sensitivity in acceleration zone location as a function of magnet current. Within the limits of the measurement uncertainty, no discernible trends are evident in the ionization zone location for the 200 V and 300 V trials for either propellant.

It is interesting to note that in the low voltage xenon trials, the acceleration zone location remains further downstream of the Hall thruster for all magnetic current values as compared to the higher voltage cases. The same is true for krypton with the exception of magnet current values $< 0.5$ A where the acceleration zone moves far enough upstream to match the location exhibited by the higher voltage trials. In general, the ionization zone location is also further downstream for the low voltage cases for both propellants.

## A. Separation Distance

Figures 18 and 19 below show the separation distance between ionization zone and acceleration zone locations. The distance is calculated as the acceleration zone location subtracted from the ionization zone location. The result is that positive values indicate an ionization zone location downstream of the acceleration zone location and the contrary for negative separation values. Unfortunately, due to the error bars, very little can be ascertained from the separation datasets. The lowest discharge voltage cases for both krypton and xenon do exhibit a decreasing separation distance as a function of decreasing magnet current for all but the lowest value of magnet current. This 'closing of the gap' between the ionization zone and acceleration zone supports the increase in voltage utilization efficiency seen in previous results. The numerical data for the separation distances are in tables 7 and 8

[b]It should be noted that trace levels of ionization will occur on either side of the bounds as defined here, but will be small in comparison

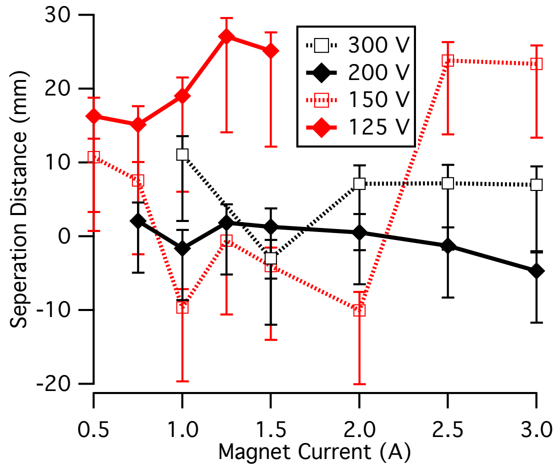


Figure 18: The separation distance between the acceleration zone and the ionization zone for krypton. Negative values indicate an ionization zone location upstream of the acceleration zone.

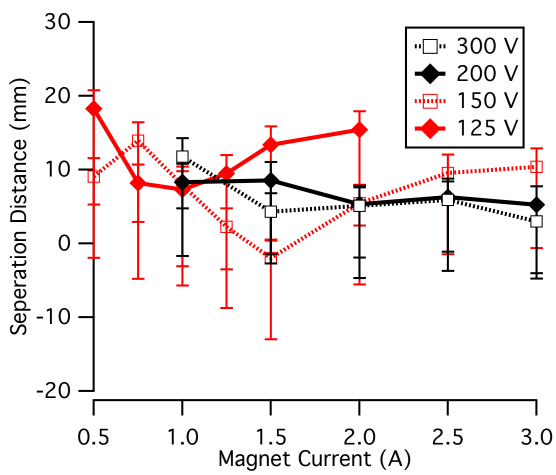


Figure 19: The separation distance between the acceleration zone and the ionization zone for xenon. Negative values indicate an ionization zone location upstream of the acceleration zone.

Table 7: The separation distance between the acceleration zone and the ionization zone for krypton. Negative values indicate an ionization zone location upstream of the acceleration zone.

| Magnet Current (A) | 125 V | 150 V | 200 V | 300 V |
|---|---|---|---|---|
| 0.50 | 16.3 | 10.7 | | |
| 0.75 | 15.3 | 7.6 | 2.1 | |
| 1.00 | 19.0 | -9.7 | -1.6 | 11.1 |
| 1.25 | 27.1 | -0.6 | 1.8 | |
| 1.50 | 25.1 | -4.0 | 1.3 | -3.0 |
| 2.00 | | -10.1 | 0.5 | 7.1 |
| 2.50 | | 23.8 | -1.3 | 7.2 |
| 3.00 | | 23.4 | -4.7 | 7.0 |

Table 8: The separation distance between the acceleration zone and the ionization zone for xenon. Negative values indicate an ionization zone location upstream of the acceleration zone.

| Magnet Current (A) | 125 V | 150 V | 200 V | 300 V |
|---|---|---|---|---|
| 0.50 | 18.3 | 9.1 | | |
| 0.75 | 8.2 | 13.9 | | |
| 1.00 | 7.3 | 7.9 | 8.3 | 11.8 |
| 1.25 | 9.5 | 2.3 | | |
| 1.50 | 13.4 | -2.0 | 8.6 | 4.3 |
| 2.00 | 15.4 | 5.5 | 5.3 | 5.1 |
| 2.50 | | 9.6 | 6.3 | 5.9 |
| 3.00 | | 10.4 | 5.3 | 3.0 |

### B. Summary

Current efficiency is the dominant loss mechanism of low voltage operation of the BPT-2000 Hall thruster. Perhaps the more interesting finding was that the voltage utilization efficiency increases as a function of decreasing magnet current for all discharge voltages. This effect was was most pronounced for lower voltages.

Among the internal probe results, it was confirmed that the ionization zone moves upstream with respect to the acceleration region with decreased magnet current for low voltages. The natural result of this is an increase in voltage utilization efficiency, which is supported by the results of earlier testing.[6,18] Decreasing the magnet current was also shown to increase the peak ion density and shift the entire ion density profile further upstream for low voltage operation. At higher voltages, the magnet current had a much smaller effect on both the location of the ionization and acceleration zones. No change in the fraction of potential drop in the acceleration region was determined as a function of magnet current for any voltage/propellant type.

The axial shift in the ionization and acceleration locations as a function of magnet current for low voltage operation was also shown to be a location shift to lower magnetic field values when compared to the higher discharge voltages at the same magnet currents. This indicates that it may be necessary for the ionization and acceleration regions to be located at lower magnetic field strengths to sustain ionization processes for low voltages. This phenomenon may be explored in detailed future work by altering the magnetic field structure, shape, number of coils etc., with the aim to increase the voltage utilization while reducing anode current.

## Acknowledgments

The author would like to thank Dr. Brad King from Orbion Space Technology for his financial and academic contributions that made this research possible.

## References

[1]Jahn, R. G., *Physics of Electric Propulsion*, Dover Publications, 1968.

[2]Goebel, D. and Katz, I., *Fundamentals of Electric Propulsion*, John Wiley and Sons, Inc., 2008.

[3]Brown, D. L., Reid, B. M., and Gallimore, A. D., "Performance Characterization and Design Verification of a 6-kW Laboratory Model Hall Thruster," *54th JANNAF Propulsion Meeting*, Denver, Colorado, May 14-17 2007.

[4]Manzella, D. and Jacobson, D., "Investigation of Low-Voltage/High-Thrust Hall Thruster Operation," *39th AIAA/ASME/SAE/ASEE Joint Propulsion Conference and Exhibit*, Vol. AIAA-2003-5004, Huntsville, Alabama, July 20-23 2003.

[5]Brown, D. L., *Investigation of Low Discharge Voltage Hall Thruster Characteristics and Evaluation of Loss Mechanisms*, Ph.D. thesis, University of Michigan, June 2009.

[6]Ross, J. L., *Probe Studies of a Hall Thruster at Low Voltages*, Ph.D. thesis, Michigan Technological University, 2011.

[7]Haas, J. M., *Low-Perturbation in Interrogation of the Internal and Near-Field Plasma Structure of a Hall Thruster Using a High-Speed Probe Positioning System*, Ph.D. thesis, University of Michigan, 2001.

[8]Haas, J. M. and Gallimore, A. D., "Development of a High-Speed, Reciprocating Electrostatic Probe System for Hall Thruster Interrogation," *Review of Scientific Instruments*, Vol. 71, No. 11, November 2000.

[9]Chen, F. F., "Lecture Notes on Langmuir Probe Diagnostics," IEEE-ICOPS, Jeju, Korea, June 5 2003.

[10]Chen, F. F., *Introduction to Plasma Physics and Controlled Fusion*, Plenum Press, 1984.

[11]Linnell, J. A. and Gallimore, A. D., "Internal Langmuir Probe Mapping of a Hall Thruster with Xenon and Krypton Prop," Vol. AIAA-2006-4470, Sacramento, California, 9-12 July 2006.

[12]Reid, B. M. and Gallimore, A. D., "Langmuir Probe Measurements in the Discharge Channel of a 6-kW Hall Thruster," *44th AIAA/ASME/SAE/ASEE Joint Propulsion Conference and Exhibit*, Vol. AIAA-2008-4920, Hartford, CT, July 20-23 2008.

[13]Kim, V., Grdlichko, D., Kozlov, V., Lazourenko, A., Popov, G., and Skrylnikov, A., "Local Plasma Parameter Measurements by Nearwall Probes Inside the SPT Accelerating Channel Under Thruster Operation with Kr," *38th AIAA/ASME/SAE/ASEE Joint Propulsion Conference & Exhibit*, Indianapolis, Indiana, July 7-10 2002.

[14]Bishaev, A. M. and Kim, V., "Local Plasma Properties in a Hall-Current Accelerator with an Extended Acceleration Zone," *Soviet Physics Technical Physics*, Vol. 23, No. 9, 1978.

[15]Esipchuk, Y. B., Morozov, A. I., Tilinin, G. N., and Trofimov, A. V., "Plasma oscillations in closed-drift accelerators with an extended acceleration zone," *Soviet Physics - Technical Physics*, Vol. 18, No. 7, 1974.

[16]Raitses, Y., Ashkenazy, J., and Appelbaum, G., "Probe measurements of plasma properties inside an experimental Hall thruster," *34th AIAA/ASME/SAE/ASEE Joint Propulsion Conference and Exhibit*, Cleveland, Ohio, July 13-15 1998.

[17]Hofer, R. R., *Development and Characterization of High-Efficiency, High-Specific Impulse Xenon Hall Thrusters*, Ph.D. thesis, University of Michigan, Ann Arbor, 2004.

[18]Ross, J. L. and King, L. B., "Efficiency Analysis of a Low Discharge Voltage Hall Thruster," *44th AIAA/ASME/SAE/ASEE Joint Propulsion Conference & Exhibit*, Hartford, CT, July 20-23 2008.